SCIENCE CHINA
Information Sciences

• RESEARCH PAPER •

August 2021, Vol. 64 182308:1–182308:10
https://doi.org/10.1007/s11432-019-2864-5

Spectrum sensing based on angular reciprocity in cognitive satellite communication system

Jiancun FAN[1,2*], Yong BAN[1], Jie LUO[1], Ying ZHANG[1] & Xinmin LUO[1]

[1]*School of Information and Communications Engineering, Xi'an Jiaotong University, Xi'an* 710049*, China;*
[2]*Science and Technology on Communication Networks Laboratory, Shijiazhuang* 050081*, China*

Received 7 October 2019/Revised 26 December 2019/Accepted 30 March 2020/Published online 2 June 2021

Abstract Satellite communication is attracting increasing attention owing to its freedom from geographical constraints. However, its spectrum resources are limited, and it is susceptible to interferences. Therefore, cognitive radio technology can be used to detect and prevent interferences as well as improve spectrum utilization. To improve the spectrum sensing performance, an angle reciprocity-based spectrum sensing (ARSS) scheme is proposed in this study. The scheme exploits the reciprocity between the known beam's central angle and the unknown signal's arrival angle, with the reciprocity controlled by the narrow characteristic of the satellite's beam owing to long-distance propagation. In this scheme, we use the beam's central angle instead of the signal's actual angle to process the received signal, and then the processed data are used as the sensing statistics for spectrum sensing. The simulation results show that the proposed ARSS scheme exhibits better satellite spectral sensing performance compared with the energy detector (ED).

Keywords satellite communications, spectrum sensing, angle reciprocity, energy detector

Citation Fan J C, Ban Y, Luo J, et al. Spectrum sensing based on angular reciprocity in cognitive satellite communication system. Sci China Inf Sci, 2021, 64(8): 182308, https://doi.org/10.1007/s11432-019-2864-5

1 Introduction

The satellite communication system has gained widespread attention because it is unaffected by geographical restrictions, ensuring wide coverage and long-distance communication [1]. Owing to these advantages, satellite and cellular communications are comprehensively integrated in the space-earth network [2]. As satellite communication traffic increases, the demand for the limited spectrum resources also increases. Therefore, cognitive radio (CR) technology is regarded as a promising technology for satellite communication systems [3] since CR technology can improve spectrum utilization and reduce interference. The research project, Cognitive Radio for Satellite Communications, launched by European scientists and other studies [4–6] shows the advantages of cognitive satellite communication networks in specific application scenarios.

To achieve simple, efficient, and reliable spectral sensing, many studies on satellite spectrum sensing have been conducted. In [7], a maximum likelihood spectrum sensing technology based on the wavelet transform in a spread spectrum cognitive satellite communication system was proposed. In [8], the neural network technology was applied for spectrum sensing research. The results of energy detector (ED), and the cyclo-stationary feature sensing algorithms are used as back propagation (BP) neural network classifier inputs. Compared with the ED algorithm, the algorithm in [8] can improve spectrum sensing performance. However, the two algorithms involve higher computational complexity and are unsuitable for the computationally constrained satellite spectrum sensing. In [9], a spectrum allocation scheme for cognitive satellite networks was proposed for improving the spectrum efficiency. This addresses the situation by considering under-utilization of the scarce spectrum resources, with the overall demands of cognitive satellite users unsatisfied. In [10], a blind spectrum sensing algorithm based on statistical tests

* Corresponding author (email: fanjc0114@gmail.com)

assuming that the interference is white was proposed. Compared with the classical spectrum sensing algorithm, this algorithm is simple and applicable, with its error detection probability obtainable. However, the actual noise spectrum is required for this algorithm.

To improve the spectrum sensing performance, multi-antenna or multi-user collaboration can be applied in CR satellite systems [11]. For example, Pierucci introduced a hybrid multiple input multiple output (MIMO) cooperative spectrum sensing scheme [12], with the MIMO technology recognized by users. The satellite is also reported to require additional on-board processing power. In [13], the spectrum sensing problem involving the dual-polarization fading channel was considered. The sensing performance of the ED algorithm was evaluated using the coexistence of satellite-to-earth links and then equal gain combining or selection combining diversity technology was adopted. In [14], a novel mathematical approach for obtaining the optimal number of samples with noise uncertainty for the energy detection method was advanced. In [15], an improved cuckoo search algorithm was proposed for spectrum sensing in cognitive satellites. This algorithm reduces the redundancy calculation and improves the convergence rate by adjusting the step size dynamically and its discovery probability. However, computing the algorithm becomes intensive owing to the search process. Therefore, Ref. [16] presented a practical low-complexity spectrum sensing algorithm to reduce the computational cost, but the power of secondary users is constrained to reduce the interference from primary users.

In this study, we investigate satellite spectrum sensing using the satellite's beam central angle when the primary user's signal and noise can be modeled as cyclic complex Gaussian distribution. Ref. [17] demonstrated that the optimal detector requires the signal direction of arrival (DOA), but in practice the DOA is unknown. Therefore, we propose an angle reciprocity-based spectrum sensing (ARSS) algorithm for satellite communication systems. This algorithm exploits the reciprocity between the known beam's central angle and the unknown actual signal's arrival angle.

The rest of this paper is organized as follows. In Section 2, we introduce the satellite spectrum sensing system model. In Section 3, we demonstrate that the satellite's beam angle is narrow according to the analysis of the actual multi-beam system, and then propose a satellite ARSS algorithm based on the beam's central angle and the actual signal's arrival angle reciprocity. In Section 4, we present results for evaluating the performance of the ARSS algorithm based on analytical derivations and simulations, and then compare the performance of the ARSS with the optimal detector and ED algorithms. The paper concludes in Section 5.

2 System model and optimal sensing scheme

In this section, we will first give the system model for multiple antenna satellite communication systems and then give the optimal sensing scheme, i.e., log-likelihood ratio spectrum sensing algorithm.

2.1 System model

Satellite communication systems often use multi-feed and multi-beam coverage technology, where the signals are focused and reflected to the feed array owing to the uniqueness of the reflection surface. Besides, the signals received by the feed array are the same signals but each feed has separate amplitude and phase gains, which is similar to multi-antenna signal reception. Therefore, the multi-feed array can be simplified into an antenna array, and then the classical methods of array signal processing can be introduced to improve the spectrum sensing performance.

Suppose that the satellite has M receiving antennas as shown in Figure 1 and there are L samples for the received signal at each antenna. Define the received signal of the ith antenna, and then we can express the received signal matrix of M antennas as $\boldsymbol{Y} = [\boldsymbol{y}_1, \boldsymbol{y}_2, \ldots, \boldsymbol{y}_L] \in C^{M\times L}$. The scene that interference exists or not can be defined as H_1 and H_0. Let $\boldsymbol{s} = [s_1, s_2, \ldots, s_L] \in C^{1\times L}$ denote the interference signal and $\boldsymbol{N} = [\boldsymbol{n}_1, \boldsymbol{n}_2, \ldots, \boldsymbol{n}_L] \in C^{M\times L}$ denote the noise signal. We assume that both interference signal and noise follow the independent complex Gaussian distribution with variances σ_s^2 and σ_n^2, respectively. The multiple antennas satellite spectrum sensing can be then expressed as the following binary hypothesis test:

$$\begin{cases} H_0 : \boldsymbol{Y} = \boldsymbol{N}, \\ H_1 : \boldsymbol{Y} = \boldsymbol{a}\boldsymbol{s} + \boldsymbol{N}, \end{cases} \tag{1}$$

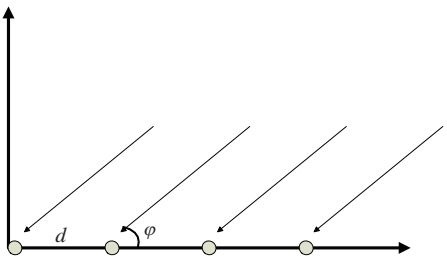

Figure 1 Satellite with multiple antennas.

where $\boldsymbol{a}$ denotes the steering vector. If the DOA of the interference signal is φ, $\boldsymbol{a}$ can be defined as

$$\boldsymbol{a}=\left[1,\ldots,\mathrm{e}^{\frac{\mathrm{j}2\pi}{\lambda}(M-1)d\cos\varphi}\right]^{\mathrm{T}}, \tag{2}$$

where d and λ are the antenna element spacing and interference signal wavelength.

2.2 Log-likelihood ratio spectrum sensing algorithm

Since there is a mature theory on log-likelihood ratio (LLR) sensing, we use the results in [17] for reference to give the following analysis.

For the hypothesis test in (1), when there is no interference, namely under hypothesis H_0, the received signal probability density function can be expressed as

$$\begin{aligned} f\left(\boldsymbol{Y}\left|H_0\right.\right)&=\prod_{l=1}^{L}\frac{1}{\left(\pi\sigma_n^2\right)^M}\exp\left\{-\frac{1}{\sigma_n^2}\boldsymbol{y}_l^{\mathrm{H}}\boldsymbol{y}_l\right\}\\ &=\frac{1}{\left(\pi\sigma_n^2\right)^{ML}}\exp\left\{-\frac{1}{\sigma_n^2}\sum_{l=1}^{L}\boldsymbol{y}_l^{\mathrm{H}}\boldsymbol{y}_l\right\}\\ &=\frac{1}{\left(\pi\sigma_n^2\right)^{ML}}\exp\left\{-\frac{\mathrm{tr}\left(\boldsymbol{Y}\boldsymbol{Y}^{\mathrm{H}}\right)}{\sigma_n^2}\right\}. \end{aligned} \tag{3}$$

By taking logarithm of the probability density function of the received signal in (3), we have

$$L_0\left(\boldsymbol{Y}\right)=\ln f\left(\boldsymbol{Y}\left|H_0\right.\right)=-\frac{\mathrm{tr}\left(\boldsymbol{Y}\boldsymbol{Y}^{\mathrm{H}}\right)}{\sigma_n^2}-ML\ln\pi-ML\ln\sigma_n^2. \tag{4}$$

Similarly, when the signal exists, under hypothesis H_1, the probability density function of the received signal is

$$\begin{aligned} f\left(\boldsymbol{Y}\left|H_1\right.\right)=&\prod_{l=1}^{L}\frac{1}{\left(\pi\right)^M\det\left(\boldsymbol{R}\right)}\exp\left\{-\boldsymbol{y}_l^{\mathrm{H}}\boldsymbol{R}^{-1}\boldsymbol{y}_l\right\}\\ =&\frac{1}{\left(\pi\right)^{ML}\det\left(\boldsymbol{R}\right)^L}\exp\left\{-\boldsymbol{y}_l^{\mathrm{H}}\boldsymbol{R}^{-1}\boldsymbol{y}_l\right\}\\ =&\frac{1}{\left(\pi\right)^{ML}\det\left(\boldsymbol{R}\right)^L}\exp\left\{-\mathrm{tr}\left(\boldsymbol{R}^{-1}\boldsymbol{Y}\boldsymbol{Y}^{\mathrm{H}}\right)\right\}, \end{aligned} \tag{5}$$

where $\boldsymbol{R}\triangleq\mathrm{E}\left[\boldsymbol{Y}\boldsymbol{Y}^{\mathrm{H}}\left|H_1\right.\right]=\sigma_s^2\boldsymbol{a}\boldsymbol{a}^{\mathrm{H}}+\sigma_n^2\boldsymbol{I}$, $\boldsymbol{R}^{-1}=\sigma_n^{-2}\boldsymbol{I}-\sigma_n^{-2}\frac{\boldsymbol{a}\boldsymbol{a}^{\mathrm{H}}}{\frac{\sigma_n^2}{\sigma_s^2}+\|\boldsymbol{a}\|^2}$. Under hypothesis H_1, by taking logarithm of the probability density function of the received signal (5), we have

$$\begin{aligned} L_1\left(\boldsymbol{Y}\right)=&-\frac{\mathrm{tr}\left(\boldsymbol{Y}\boldsymbol{Y}^{\mathrm{H}}\right)}{\sigma_n^2}+\frac{\left\|\boldsymbol{a}^{\mathrm{H}}\boldsymbol{Y}\right\|^2}{(\frac{\sigma_n^2}{\sigma_s^2}+\left\|\boldsymbol{a}\right\|^2)\sigma_n^2}\\ &-ML\ln\pi-ML\ln\sigma_n^2-L\ln\left(\frac{\sigma_s^2}{\sigma_n^2}\|\boldsymbol{a}\|^2+1\right). \end{aligned} \tag{6}$$

We define the logarithm of likelihood ratio function as

$$\begin{aligned}\mathrm{LLR}=&\ln\frac{f\left(\boldsymbol{Y}\left|H_1\right.\right)}{f\left(\boldsymbol{Y}\left|H_0\right.\right)}\\=&\ln f\left(\boldsymbol{Y}\left|H_1\right.\right)-\ln f\left(\boldsymbol{Y}\left|H_0\right.\right)\\=&\frac{\left\|\boldsymbol{a}^{\mathrm{H}}\boldsymbol{Y}\right\|^2}{\sigma_n^2(\frac{\sigma_n^2}{\sigma_s^2}+\left\|\boldsymbol{a}\right\|^2)}-L\ln\left(\frac{\sigma_s^2}{\sigma_n^2}\left\|\boldsymbol{a}\right\|^2+1\right).\end{aligned}\tag{7}$$

Therefore, the spectrum sensing decision problem can be transformed into

$$\mathrm{LLR}=\frac{\left\|\boldsymbol{a}^{\mathrm{H}}\boldsymbol{Y}\right\|^2}{\sigma_n^2(\frac{\sigma_n^2}{\sigma_s^2}+\left\|\boldsymbol{a}\right\|^2)}-L\ln\left(\frac{\sigma_s^2}{\sigma_n^2}\left\|\boldsymbol{a}\right\|^2+1\right)\underset{H_0}{\overset{H_1}{\gtrless}}\gamma_{\mathrm{LLR1}}.\tag{8}$$

When the DOA of the interference signal φ is fully known, that is, the steering vector $\boldsymbol{a}$ is known, the steering vector can be used to preprocess the received signal, and the energy of the data after the preprocessing can be taken as the perception statistics of spectral perception. At this point, the decision problem can be transformed into

$$T_{\mathrm{LLR}}=\left|\left|\boldsymbol{a}^{\mathrm{H}}\boldsymbol{Y}\right|\right|^2\underset{H_0}{\overset{H_1}{\gtrless}}\gamma_{\mathrm{LLR}}.\tag{9}$$

The relationship between threshold γ_{LLR1} and γ_{LLR} can be expressed as

$$\gamma_{\mathrm{LLR}}=\sigma_n^2\left(\frac{\sigma_n^2}{\sigma_s^2}+\left\|\boldsymbol{a}\right\|^2\right)\left(L\ln\left(\frac{\sigma_s^2}{\sigma_n^2}\left\|\boldsymbol{a}\right\|^2+1\right)+\gamma_{\mathrm{LLR1}}\right).\tag{10}$$

Under hypothesis H_0, the steering vector $\boldsymbol{a}$ is used to preprocess the received signal $\boldsymbol{Y}$, and the data distribution after preprocessing is satisfied:

$$H_0:\boldsymbol{a}^{\mathrm{H}}\boldsymbol{Y}\sim CN\left(0,\sigma_n^2\left\|\boldsymbol{a}\right\|^2\boldsymbol{I}_L\right).\tag{11}$$

Then we can get the following distribution of perception statistics under hypothesis H_0:

$$\frac{T_{\mathrm{LLR}}}{\sigma_n^2\left\|\boldsymbol{a}\right\|^2}=\frac{\left\|\boldsymbol{a}^{\mathrm{H}}\boldsymbol{Y}\right\|^2}{\sigma_n^2\left\|\boldsymbol{a}\right\|^2}\sim\chi_{2L}^2.\tag{12}$$

According to the above distribution, its false alarm probability P_f can be expressed as

$$P_f=P\left(T_{\mathrm{LLR}}>\gamma_{\mathrm{LLR}}\left|H_0\right.\right)=\frac{\Gamma(L,\frac{\gamma_{\mathrm{LLR}}}{\sigma_n^2\left\|\boldsymbol{a}\right\|^2})}{\Gamma\left(L\right)},\tag{13}$$

where $\Gamma\left(L,x\right)=\int_x^\infty t^{L-1}\mathrm{e}^{-t}\mathrm{d}t$, $\Gamma\left(L\right)=\int_0^\infty t^{L-1}\mathrm{e}^{-t}\mathrm{d}t$. In general, the sampling length of a single antenna L can be regarded as known. In this case, $\Gamma\left(L,x\right)$ monotone decreases; that is, it decreases with x increases. Similarly, under hypothesis H_1, the data distribution after preprocessing is satisfied:

$$H_1:\boldsymbol{a}^{\mathrm{H}}\boldsymbol{Y}\sim CN\left(0,\left\|\boldsymbol{a}\right\|^2\left(\sigma_s^2\left\|\boldsymbol{a}\right\|^2+\sigma_n^2\right)\boldsymbol{I}_L\right).\tag{14}$$

Then we can get the distribution of perception statistics under hypothesis H_1:

$$\frac{T_{\mathrm{LLR}}}{\left\|\boldsymbol{a}\right\|^2(\sigma_s^2\left\|\boldsymbol{a}\right\|^2+\sigma_n^2)}=\frac{\left\|\boldsymbol{a}^{\mathrm{H}}\boldsymbol{Y}\right\|^2}{\left\|\boldsymbol{a}\right\|^2(\sigma_s^2\left\|\boldsymbol{a}\right\|^2+\sigma_n^2)}\sim\chi_{2L}^2.\tag{15}$$

The detection probability P_d can be expressed as

$$P_d=P\left(T_{\mathrm{LLR}}>\gamma_{\mathrm{LLR}}\left|H_1\right.\right)=\frac{\Gamma(L,\frac{\gamma_{\mathrm{LLR}}}{\left\|\boldsymbol{a}\right\|^2(\sigma_s^2\left\|\boldsymbol{a}\right\|^2+\sigma_n^2)})}{\Gamma\left(L\right)}.\tag{16}$$

However, for the above optimal detector, the DOA of interference is assumed to be known, but in practice it is unknown. Therefore, we have to design a spectrum sensing scheme with unknown DOA information by using the angle reciprocity.

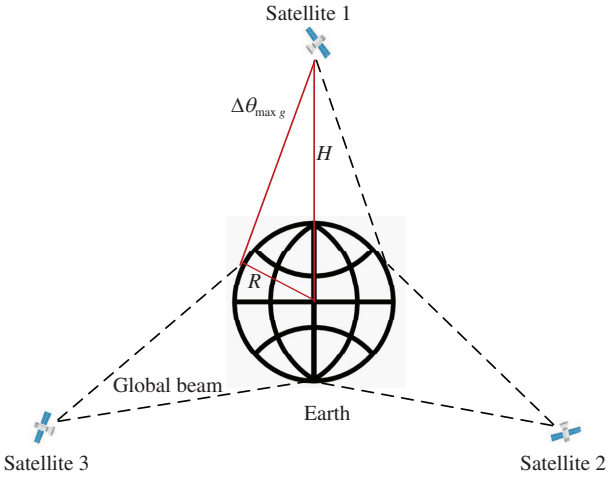

Figure 2 (Color online) Inmarsat-4 satellite global beam angular.

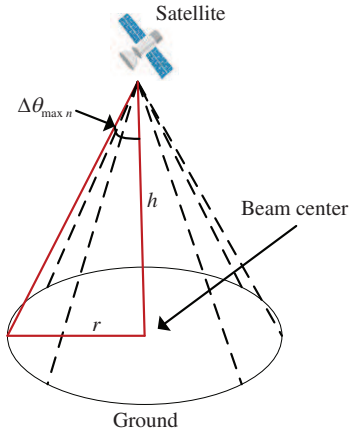

Figure 3 (Color online) Inmarsat-4 satellite narrow spot beam angular.

3 Angular reciprocity-based spectrum sensing

In this section, we first analyze the reciprocity of satellite beam angle, and then give angular reciprocity-based spectrum sensing algorithm. Finally, we analyze the performance of the proposed and optimize the number of antennas.

3.1 Satellite beam angle analysis

Let $\Delta\theta$ denote the offset between the actual angle and beam central angle, and $\Delta\theta_{\max}$ is the maximum angle offset within the beam. Taking Inmarsat-4 as an example, a single satellite of the system has a feed array consisting of 120 feeds, forming one global beam, 19 wide beams and 228 narrow spot beams. We assume that the world can be fully covered by three satellites with global beams. The angle offset of the global beam can be shown in Figure 2, so we can get the maximum angle offset of the global beam as follows:

$$\Delta\theta_{\max g} = \arcsin\left(\frac{R}{H}\right), \tag{17}$$

where R and H are the radius of the earth and the distance from Satellite to Earth's geocentric. The radius of the earth is about 6371 km, and the synchronous satellite is 35786 km away from the ground. The maximum angle offset of the global beam of the Inmarsat-4 satellite is obtained as 8.6922°.

However, the Inmarsat-4 transmits data mainly through narrow spot beams. The maximum angle offset of the narrow spot beam is shown in Figure 3 and can be determined as

$$\Delta\theta_{\max n} = \arctan\left(\frac{r}{h}\right), \tag{18}$$

where r and h are the radius of the narrow spot beam and the distance from satellite to the ground. Assuming that all narrow-beams of the three satellites are turned on, and then the whole world can be covered. In this case, the maximum angle offset of the Inmarsat-4 satellite narrow spot beam is 0.78°. In order to improve the system capacity, the existing multi-feed and multi-beam synchronous satellite system mostly adopts narrow spot beam technology. It has been estimated that, in the existing synchronous satellite communication system, the maximum angle offset of the Garuda satellite is about 0.7226°, the maximum angle offset of the US TerreStar satellite system is about 0.5967°, and the maximum angle offset of China Tiantong satellite is about 0.5604°.

Through the above estimation, it can be found that the satellite narrow spot beam angle is small and there is a small difference between the DOA of the signal in the beam and the known beam central angle. Therefore, we can use this feature to improve satellite spectrum sensing performance.

3.2 Angular reciprocity-based sensing algorithm

Define the angle offset between the actual DOA and the beam central angle ω as $\Delta\theta$, and then we can get the actual steering vector $\boldsymbol{a}$ as

$$\boldsymbol{a}=\left[1,\mathrm{e}^{\frac{\mathrm{j}2\pi}{\lambda}d\cos(\omega+\Delta\theta)},\ldots,\mathrm{e}^{\frac{\mathrm{j}2\pi}{\lambda}(M-1)d\cos(\omega+\Delta\theta)}\right]^{\mathrm{T}}. \tag{19}$$

When the narrow beam coverage of the satellite is determined, the beam central angle is equivalently known. In this case, the narrower the beam of the satellite communication system is, the smaller the offset between the beam central angle and the signal arrival angle is. According to the reciprocity of the angle, if the beam central angle is used in the preprocessing for the received signals, the preprocessing matrix can be expressed as

$$\boldsymbol{b}=\left[1,\mathrm{e}^{\frac{\mathrm{j}2\pi}{\lambda}d\cos\omega},\ldots,\mathrm{e}^{\frac{\mathrm{j}2\pi}{\lambda}(M-1)d\cos\omega}\right]^{\mathrm{T}}. \tag{20}$$

Then the test statistic can be expressed as

$$T_{\mathrm{ARSS}}=||\boldsymbol{b}^{H}\boldsymbol{Y}||^{2}\underset{H_0}{\overset{H_1}{\gtrless}}\gamma_{\mathrm{ARSS}}. \tag{21}$$

Similar to (11) and (14), the statistical distribution of the signal after preprocessing is satisfied as follows:

$$H_0:\boldsymbol{b}^{\mathrm{H}}\boldsymbol{Y}\sim CN\left(0,\sigma_n^2\|\boldsymbol{b}\|^2\boldsymbol{I}_L\right), \tag{22}$$

$$H_1:\boldsymbol{b}^{\mathrm{H}}\boldsymbol{Y}\sim CN\left(0,\left(\sigma_n^2\|\boldsymbol{b}\|^2+\sigma_s^2\left|(\boldsymbol{b})^{\mathrm{H}}\boldsymbol{a}\right|^2\right)\boldsymbol{I}_L\right). \tag{23}$$

In this case, the false alarm probability P_f and detection probability P_d of the ARSS algorithm are as follows:

$$P_f=P\left(T_{\mathrm{ARSS}}>\gamma_{\mathrm{ARSS}}\,|H_0\right)=\frac{\Gamma(L,\frac{\gamma_{\mathrm{ARSS}}}{\sigma_n^2\|\boldsymbol{b}\|^2})}{\Gamma\left(L\right)}, \tag{24}$$

$$P_d=P\left(T_{\mathrm{ARSS}}>\gamma_{\mathrm{ARSS}}\,|H_1\right)=\frac{\Gamma(L,\frac{\gamma_{\mathrm{ARSS}}}{(\sigma_n^2\|\boldsymbol{b}\|^2+\sigma_s^2|\boldsymbol{b}^{\mathrm{H}}\boldsymbol{a}|^2)})}{\Gamma\left(L\right)}, \tag{25}$$

where the probability of missed detection $P_m=1-P_d$.

3.3 Performance of angle reciprocity algorithm

From (24) and (25), we investigate the performance of the ARSS algorithm. We can know that the sensing threshold is still determined by the noise variance σ_n^2, the single antenna sampling length L, the number of antennas M, and the false alarm probability P_f. And the probability of missed detection of the ARSS algorithm is determined by the sensing threshold γ_{ARSS}, single antenna sample number L, noise variance σ_n^2, signal variance σ_s^2, preprocessed vector norm $\|\boldsymbol{b}\|^2$, and norm of preprocessing matrix and steering vector product $|\boldsymbol{b}^{\mathrm{H}}\boldsymbol{a}|^2$.

When the single antenna sampling length and the false alarm probability are fixed, we can get the sensing threshold according to the Neyman-Pearson criterion, and $\frac{\gamma_{\mathrm{ARSS}}}{\sigma_n^2\|\boldsymbol{b}\|^2}=T$ is a fixed value. At this time, the probability of missed detection of the ARSS algorithm is determined by the following formula:

$$\frac{\gamma_{\mathrm{ARSS}}}{(\sigma_n^2\|\boldsymbol{b}\|^2+\sigma_s^2|\boldsymbol{b}^{\mathrm{H}}\boldsymbol{a}|^2)}=\frac{T}{(1+\mathrm{SNR}\frac{|\boldsymbol{b}^{\mathrm{H}}\boldsymbol{a}|^2}{\|\boldsymbol{b}\|^2})}. \tag{26}$$

The missed detection probability of the ARSS algorithm is mainly affected by two factors. The first part is the signal-to-noise ratio (SNR) at the antenna. Another part is the ratio between the conjugated transpose of the preprocessing matrix formed by the beam center angle and the square of the product of the steering vector product, i.e., $\frac{|\boldsymbol{b}^{\mathrm{H}}\boldsymbol{a}|^2}{\|\boldsymbol{b}\|^2}$. The smaller the product of these two parts, the larger the

probability of missed detection and the worse the sensing performance will be. Taking a one-dimensional uniform linear array as an example, the square of the steering vector is equal to the number of antennas,

$$\|\boldsymbol{b}\|^2 = M. \tag{27}$$

Then the second part can be written as

$$\begin{aligned}\frac{|\boldsymbol{b}^{\mathrm{H}}\boldsymbol{a}|^2}{\|\boldsymbol{b}\|^2} &= \frac{1}{M}\left|1+\sum_{i=1}^{M-1}\mathrm{e}^{\frac{\mathrm{j}2\pi d}{\lambda}d\times i\times[\cos(\omega+\Delta\theta)-\cos\omega]}\right|^2\\ &= \frac{1}{M}\left|\frac{1-\mathrm{e}^{M\frac{\mathrm{j}2\pi d}{\lambda}[\cos(\omega+\Delta\theta)-\cos\omega]}}{1-\mathrm{e}^{\frac{\mathrm{j}2\pi d}{\lambda}\times[\cos(\omega+\Delta\theta)-\cos\omega]}}\right|^2.\end{aligned} \tag{28}$$

When the SNR is low, the probability of missed detection is mainly determined by the SNR. On the contrary, the performance is mainly determined by the angle offset and the number of antennas M.

In an actual system [18], with the increase of the number of antennas, the beam will be narrower, the maximum beam gain will be larger, and the gain will be more sensitive to the angle offset. On the other hand, the fewer the number of antennas, the wider the beam, and the smaller the maximum beam gain that can be obtained, the less sensitive the gain is to the angular offset. Therefore, there should be an optimal antenna number corresponding to the different angular offsets. From (28), the optimal number of antennas can be got by using the following optimization problem:

$$M_{\mathrm{opt}} = \max_M \frac{1}{M}\left|\frac{1-\mathrm{e}^{M\frac{\mathrm{j}2\pi d}{\lambda}[\cos(\omega+\Delta\theta)-\cos\omega]}}{1-\mathrm{e}^{\frac{\mathrm{j}2\pi d}{\lambda}\times[\cos(\omega+\Delta\theta)-\cos\omega]}}\right|^2. \tag{29}$$

Because of the long distance between the satellite and the earth, it can be assumed that the satellite is vertically covering the ground, and the central angle of the beam can be regarded as $\omega = 90^\circ$. Owing to the narrow satellite beam angle, the maximum angle offset is small, and we can get $\sin(\Delta\theta) \doteq \Delta\theta$. So the optimal number of antennas can be achieved by

$$\begin{aligned}M_{\mathrm{opt}} &= \max_M \frac{1}{M}\left|\frac{1-\mathrm{e}^{M\frac{\mathrm{j}2\pi d}{\lambda}[\cos(\omega+\Delta\theta)-\cos\omega]}}{1-\mathrm{e}^{\frac{\mathrm{j}2\pi d}{\lambda}\times[\cos(\omega+\Delta\theta)-\cos\omega]}}\right|^2\\ &= \max_M \frac{1}{M}\left|\frac{1-\mathrm{e}^{\frac{\mathrm{j}2\pi dM}{\lambda}[-\sin\Delta\theta]}}{1-\mathrm{e}^{\frac{\mathrm{j}2\pi d}{\lambda}[-\sin\Delta\theta]}}\right|^2 = \frac{1}{M}\left|\frac{1-\mathrm{e}^{\frac{\mathrm{j}2\pi dM}{\lambda}[-\Delta\theta]}}{1-\mathrm{e}^{\frac{\mathrm{j}2\pi d}{\lambda}[-\Delta\theta]}}\right|^2\\ &= \max_M \frac{1}{M}\left|\frac{1-\cos\left(\frac{2\pi dM\Delta\theta}{\lambda}\right)+\mathrm{j}\sin\left(\frac{2\pi dM\Delta\theta}{\lambda}\right)}{1-\cos\left(\frac{2\pi d\Delta\theta}{\lambda}\right)+\mathrm{j}\sin\left(\frac{2\pi d\Delta\theta}{\lambda}\right)}\right|^2\\ &= \max_M \frac{1}{M}\frac{1-\cos\left(\frac{2\pi dM\Delta\theta}{\lambda}\right)}{1-\cos\left(\frac{2\pi d\Delta\theta}{\lambda}\right)}.\end{aligned} \tag{30}$$

Figure 4 shows the variation of the optimal number of antennas with different angular offsets $\Delta\theta$. When the central angle of the beam is 90°, it can be seen from the curve that the optimal antenna number is large when the $\Delta\theta$ is small. When $\Delta\theta$ is small, increasing the number of antennas can improve the sensing performance, but when $\Delta\theta$ is large, increasing the number of antennas may reduce the perceptual performance. Therefore, it is necessary to select the number of antennas to be perceived according to the optimal number of antennas obtained by the formula (30) and the maximum number of antennas that the system can provide.

4 Simulation results

In this section, we evaluate the performance of the ARSS algorithm by computer simulation results. In the simulation, we exploit the uniform linear array with half wavelength antenna space and assume that the sampling length at each antenna L is 4. The other parameters will be set according to the different simulation requirements in the following.

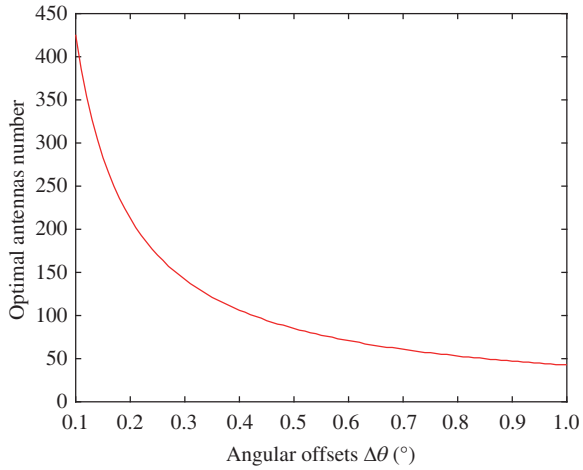

Figure 4 (Color online) The optimal antennas varies the angular offset $\Delta\theta$ of actual DOA and beam center.

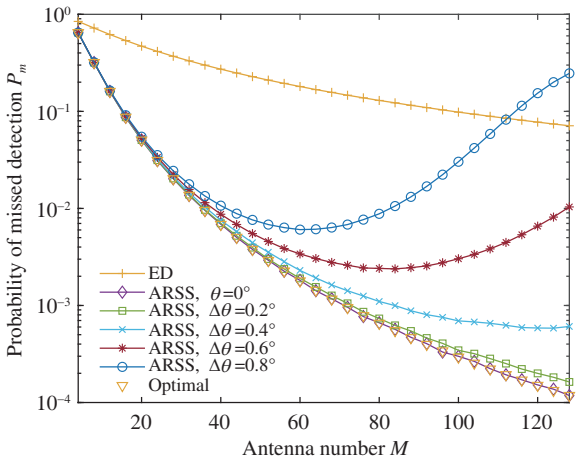

Figure 5 (Color online) Under different angular offset $\Delta\theta$, the probability of missed detection of the ARSS algorithm, the ED algorithm and the optimal algorithm versus antenna number M, for $P_f = 0.01$, $L = 0.01$ and SNR $= -5$ dB.

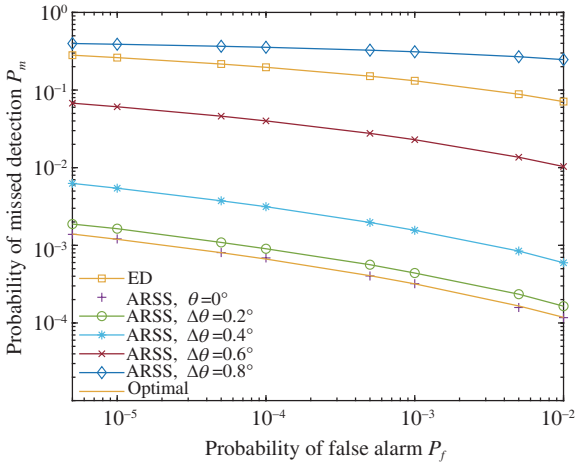

Figure 6 (Color online) Under different angular offset $\Delta\theta$, the probability of missed detection of the ARSS algorithm, the ED algorithm and the optimal algorithm versus probability of false alarm P_f, for $M = 128$, $L = 4$ and SNR $= -5$ dB.

Figure 5 depicts the probability of missed detection P_m of the optimal algorithm, the proposed ARSS algorithm and ED versus the number of antenna M, for $P_f = 0.01$ and SNR $= -5$ dB. As can be observed, when $M \leqslant 60$, by increasing M the performance of the ARSS algorithm improves and is always better than ED. When $\Delta\theta$ is small, for example when $\Delta\theta \leqslant 0.4°$, as M increases, P_m becomes smaller. But when $\Delta\theta$ is large, for example when $\Delta\theta = 0.6°$ and $M \geqslant 78$ or $\Delta\theta = 0.8°$ and $M \geqslant 58$, as M increases, P_m may become larger. However, in the same situation P_m of ED becomes smaller as M increases, P_m of ARSS algorithm is larger than ED when $\Delta\theta \geqslant 0.8°$ and $M \geqslant 116$. Therefore, it is not that the bigger M, the better the performance, so we need to choose the appropriate number of antenna according to the different $\Delta\theta$. As can be seen from Figure 5, when $\Delta\theta$ is 0.6° and 0.8°, the best M is 74 and 54, respectively, and when $\Delta\theta$ is less than 0.4°, the larger M is, the better, which are consistent with the results of (30) and Figure 4.

Figure 6 depicts the probability of missed detection P_m versus probability of the false alarm P_f and the parameters are set as $M = 128$ and SNR $= -5$ dB. Regardless of the ED or the ARSS algorithm, the overall trend is that P_m decreases with the increase of P_f. When $\Delta\theta = 0.8°$, the perceived performance of the ARSS algorithm is weaker than ED. The reason is that when $M = 128$, the increase of $\Delta\theta$ causes $\frac{|\boldsymbol{b}^{\mathrm{H}}\boldsymbol{a}|^2}{\|\boldsymbol{b}\|^2}$ to be smaller. As $\Delta\theta$ continues to increase, the perceived performance gap of the ARSS algorithm is growing.

In Figure 7, we compare the proposed ARSS algorithm under different angular with the optimal detector

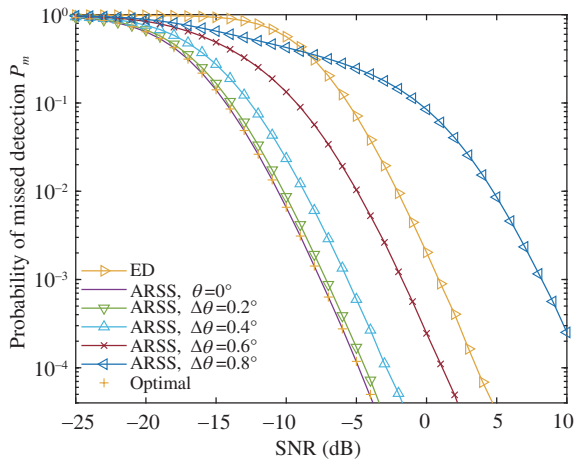

Figure 7 (Color online) Under different angular offset $\Delta\theta$, the probability of missed detection of the ARSS algorithm, the ED algorithm, and the optimal algorithm versus SNR, for $P_f = 0.01$, $L = 4$ and $M = 128$.

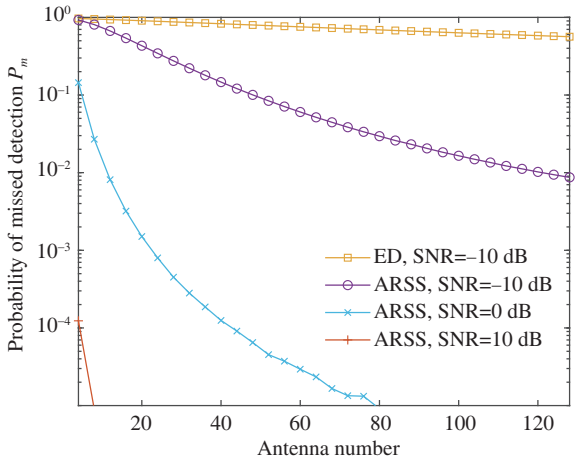

Figure 8 (Color online) Under different signal-to-noise ratio SNR, the probability of missed detection of the ARSS algorithm, the ED algorithm and the optimal algorithm versus antenna number M, for $P_f = 0.01$, $L = 4$ and $\Delta\theta = 0.2°$.

and ED versus SNR at a false alarm rate of $P_f = 0.01$ and $M = 128$. As can be observed, the performances of three algorithms have improved as SNR increases. As $\Delta\theta$ increases, the ARSS algorithm has evident differences in sensing performance. For example, when SNR $\leqslant -8$ dB, the detection performance of the ARSS algorithm is better than that of the ED algorithm. However, when SNR $\geqslant -8$ dB and $\Delta\theta = 0.8°$, the sensing performance of ARSS algorithm is worse than that of the ED algorithm. Therefore, the influence of $\Delta\theta$ on the algorithm performance needs to be considered in the case of high SNR, which is consistent with the theory obtained by the above theoretical analysis.

In Figure 8, we can know that the probability of missed detection P_m varies with the number of antennas M under different SNR, for $P_f = 0.01$, $L = 4$ and $\Delta\theta = 0.2°$. Under different SNR, when $\Delta\theta = 0.2°$, the performances of ARSS algorithm have improved with M increasing, which is consistent with the analysis results of Figure 5. With the increase of SNR, the change rate of the P_m curve also increases with the increase of M. It is worth noting that when the amount of change in $\frac{|\boldsymbol{b}^{\mathrm{H}}\boldsymbol{a}|^2}{\|\boldsymbol{b}\|^2}$ is the same, the larger SNR, the larger P_m becomes. When $\Delta\theta = 0.2°$, if M is small, the perceived performance can be improved quickly by increasing M; if M is large, the change of M has little effect on the P_m value, and the change speed of the P_m curve becomes mild. At this time, if you want to improve the perceptual performance quickly, the best way is to increase the SNR at the cognitive user.

5 Conclusion

In this study, we proposed an ARSS spectral sensing algorithm for a cognitive satellite equipped with multiple feeds. First, we demonstrated that satellite communication systems with many narrow spot beams were characterized by small beam angles. Further, we proposed the ARSS algorithm exploiting the reciprocity between the unknown actual signal angle and the known beam's central angle. From theoretical analysis of the ARSS algorithm, we obtained expressions for the false alarm probability, missed detection probability and the optimal number of antennas. The simulation results showed that the proposed ARSS algorithm performed better than the ED algorithm and was almost identical to the optimal detector at low SNR. At high SNR, the ARSS algorithm still performed better than the ED algorithm for low angle offset. At high angle offset, the ARSS algorithm yielded better performance than the ED algorithm at the optimal antenna number. Therefore, the proposed ARSS algorithm ensures better satellite communication performance through appropriate parameter configuration.

Acknowledgements This work was partially supported by National Natural Science Foundation of China (Grants No. 61671367), Key Research and Development Plan of Shaanxi Province (Grant No. 2018GY-003), Research Foundation of Science and Technology on Communication Networks Laboratory, Postdoctoral Science Foundation of Shanxi Province, and Fundamental Research Funds for the Central Universities.

References

1 Zhang X, Wang J, Jiang C, et al. Robust beamforming for multibeam satellite communication in the face of phase perturbations. IEEE Trans Veh Technol, 2019, 68: 3043–3047
2 Papathanassiou A, Salkintzis A K, Mathiopoulos P T. A comparison study of the uplink performance of W-CDMA and OFDM for mobile multimedia communications via LEO satellites. IEEE Pers Commun, 2001, 8: 35–43
3 Zeng Y, Liang Y. Maximum-minimum eigenvalue detection for cognitive radio. In: Proceedings of 2007 IEEE 18th International Symposium on Personal, Indoor and Mobile Radio Communications, 2007. 1–5
4 Liolis K, Schlueter G, Krause J, et al. Cognitive radio scenarios for satellite communications: the corasat approach. In: Proceedings of 2013 Future Network Mobile Summit, 2013. 1–10
5 Chae S H, Jeong C, Lee K. Cooperative communication for cognitive satellite networks. IEEE Trans Commun, 2018, 66: 5140–5154
6 Tarchi D, Guidotti A, Icolari V, et al. Technical challenges for cognitive radio application in satellite communications. In: Proceedings of 2014 9th International Conference on Cognitive Radio Oriented Wireless Networks and Communications (CROWNCOM), 2014. 136–142
7 Li H, Li J. Wavelet transforms detection of spectrum sensing in the space network. In: Proceedings of 2015 Science and Information Conference (SAI), 2015. 978–984
8 Wu Z, Luo M, Yin Z, et al. Research of spectrum sensing based on ANN algorithm. In: Proceedings of the 4th International Conference on Instrumentation and Measurement, Computer, Communication and Control, 2014. 493–496
9 Li F, Liu X, Lam K Y, et al. Spectrum allocation with asymmetric monopoly model for multibeam-based cognitive satellite networks. IEEE Access, 2018, 6: 9713–9722
10 Sujatmoko K, Wibisono G, Gunawan D. Notice of violation of ieee publication principles: blind spectrum sensing for cognitive radio using discriminant analysis. In: Proceedings of 2012 IEEE International Conference on Communication, Networks and Satellite (ComNetSat), 2012. 40–43
11 Jia M, Zhang X, Gu X, et al. Interbeam interference constrained resource allocation for shared spectrum multibeam satellite communication systems. IEEE Internet Things J, 2019, 6: 6052–6059
12 Pierucci L, Fantacci R. Mimo cooperative spectrum sensing in hybrid satellite/terrestrial scenario. In: Proceedings of 2015 IEEE International Conference on Communication Workshop (ICCW), 2015. 1617–1622
13 Sharma S K, Chatzinotas S, Ottersten B. Spectrum sensing in dual polarized fading channels for cognitive satcoms. In: Proceedings of 2012 IEEE Global Communications Conference (GLOBECOM), 2012. 3419–3424
14 Mahendru G, Shukla A, Banerjee P. A novel mathematical model for energy detection based spectrum sensing in cognitive radio networks. Wirel Pers Commun, 2020, 110: 1237–1249
15 Yuan W, Yang M, Guo Q, et al. Improved cuckoo search algorithm for spectrum sensing in sparse satellite cognitive systems. In: Proceedings of 2016 IEEE 84th Vehicular Technology Conference (VTC-Fall), 2016. 1–5
16 Wang X, Ekin S, Serpedin E. Joint spectrum sensing and resource allocation in multi-band-multi-user cognitive radio networks. IEEE Trans Commun, 2018, 66: 3281–3293
17 Taherpour A, Nasiri-Kenari M, Gazor S. Multiple antenna spectrum sensing in cognitive radios. IEEE Trans Wirel Commun, 2010, 9: 814–823
18 Fan J, Han L, Luo X, et al. Beamwidth design for beam scanning in millimeter-wave cellular networks. IEEE Trans Veh Technol, 2020, 69: 1111–1116